Ultrahigh Passive Cooling Power in Hydrogel with Rationally Designed Optofluidic Properties

Jipeng Fei, Di Han, Xuan Zhang, Ke Li, Nicolas Lavielle, Kai Zhou, Xingli Wang, Jun Yan Tan, Jianwei Zhong, Man Pun Wan, et al.

NANO LETTERS

pubs.acs.org/NanoLett Letter

Ultrahigh Passive Cooling Power in Hydrogel with Rationally Designed Optofluidic Properties

Jipeng Fei,△ Di Han,△ Xuan Zhang,△ Ke Li,△ Nicolas Lavielle, Kai Zhou, Xingli Wang, Jun Yan Tan, Jianwei Zhong, Man Pun Wan, Elyes Nefzaoui, Tarik Bourouina, Shuzhou Li, Bing Feng Ng, Lili Cai, and Hong Li*

Cite This: https://doi.org/10.1021/acs.nanolett.3c03694 Read Online

ACCESS | Metrics & More | Article Recommendations | Supporting Information

ABSTRACT: The cooling power of a radiative cooler is more than halved in the tropics, e.g., Singapore, because of its harsh weather conditions including high humidity (84% on average), strong downward atmospheric radiation (~40% higher than elsewhere), abundant rainfall, and intense solar radiation (up to 1200 W/m^2 with ~58% higher UV irradiation). So far, there has been no report of daytime radiative cooling that well achieves effective subambient cooling. Herein, through integrated passive cooling strategies in a hydrogel with desirable optofluidic properties, we demonstrate stable subambient (4−8 °C) cooling even under the strongest solar radiation in Singapore. The integrated passive cooler achieves an ultrahigh cooling power of ~350 W/m^2, 6−10 times higher than a radiative cooler in a tropical climate. An in situ study of radiative cooling with various hydration levels and ambient humidity is conducted to understand the interaction between radiation and evaporative cooling. This work provides insights for the design of an integrated cooler for various climates.

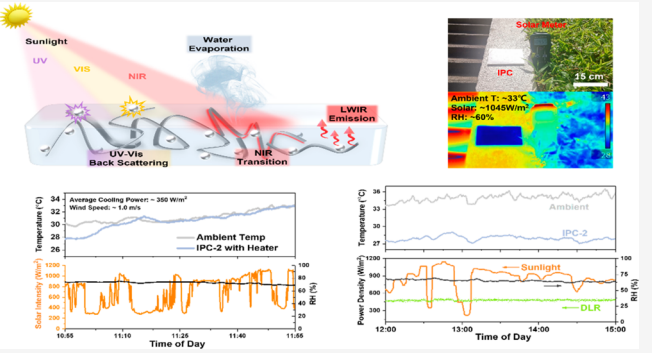

KEYWORDS: *optofluidic design, passive cooling, radiative cooling, hydrogel, integrated cooling structure*

To achieve a sustainable development, COP26 set the ambitious target of net-zero carbon emission by the middle of the century, which urgently calls for low-carbon technologies.[1−4] Energy-related carbon emissions totaled 31.5 billion metric tons in 2020. Active cooling consumes a considerable amount of energy, especially in the summer season of most countries and in all seasons of tropical zones such as Singapore. For instance, cooling is responsible for over 60% of the electricity consumption in nonresidential buildings in Singapore, where 95% of the electricity comes from burning natural gas.[5] Thus, developing an energy-saving cooling method is crucial for achieving the COP26 goal of carbon neutrality and sustainability.

Passive cooling, free of energy consumption, can be realized by various strategies such as radiative cooling, evaporative cooling, high solar reflection, heat insulation, etc.[6] Recently, passive radiative coolers (PRCs) have attracted ever-increasing attention, which achieve cooling by emitting long-wave infrared (LWIR) radiation to outer space through the atmospheric window (8−13 μm).[7−12] Daytime subambient cooling in many temperate regions is achievable when the PRC has an ultrahigh solar reflectivity (R_{solar}) of more than 94% to greatly reduce solar heat gain.[7] However, effective thermal radiation to outer space in the tropical region is significantly impeded by the high relative humidity (RH) and abundant thick clouds, leading to more than halved cooling power,[13] as evidenced by the exceptionally high downwelling radiation from the sky (up to 500 W/m^2). As a result, effective cooling power through the atmospheric window is significantly lower (down to <15 W/m^2) than its theoretical upper limit of ~150 W/m^2.[14] Thus far, subambient radiative cooling has hardly been achieved in a tropical climate with >1000 W/m^2 solar irradiance even using the best reported PRC ($R_{solar} \approx 97\%$ and long-wavelength infrared emissivity $E_{LWIR} \approx 96\%$).[15]

As a very effective method, evaporative cooling has been employed from ancient times (e.g., an Egyptian qullah) to modern days (e.g., a Zeer fridge in Africa). However, it is far from providing optimal cooling in terms of cooling power per unit of water consumption. Very recently, a combination of evaporative and radiative cooling has been attempted in a

Received: September 26, 2023
Revised: November 20, 2023
Accepted: November 20, 2023

https://doi.org/10.1021/acs.nanolett.3c03694
Nano Lett. XXXX, XXX, XXX−XXX

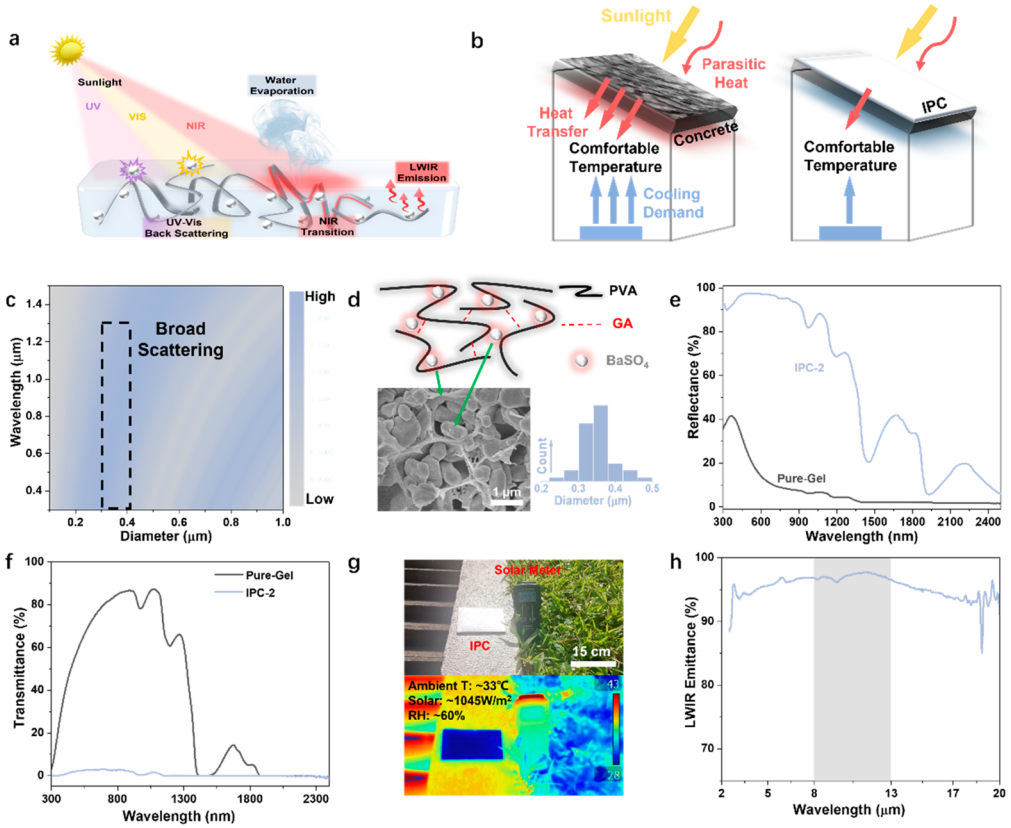

Figure 1. IPC design and characterizations. (a) Schematic illustration of cooling mechanisms. (b) Illustration of active cooling demand (ACD) difference with bare (left) and IPC-covered (right) concretes. (c) Simulated scattering efficiency (300−1300 nm) with varying BSP sizes. (d) Structural illustration (upper) and scanning electron microscopy image (lower left, scale bar is 1 μm) of IPC and BSP size distribution (lower right). (e) Solar reflectance and (f) transmittance spectra of pure-Gel and IPC-2. (g) Optical (upper) and IR image (lower) of IPC-2 under sunlight taken after 30 min stabilization. (h) LWIR emittance spectrum of IPC-2. The shaded area labels the atmospheric window wavelength range.

double-layer hydrogel−hydrophobic PRC structure.[16] A cooling power of ∼250 W/m^2 has been achieved, which is much higher than that of an ideal radiative cooler. However, such a design has a few outstanding issues to address. Most importantly, the cooling power is not optimized due to the reduction of evaporative surface arising from the capping PRC layer. Moreover, the structural integrity caused by a problematic interfacial contact between the hydrated polymer (hydrogel) and the hydrophobic radiative cooling layer, especially upon severe water loss, needs to be improved. Additionally, the multilayer structure, which has more complex fabrication and coating processes than those of a single composite, limits its application.

Nevertheless, when both radiative cooling and evaporative cooling are integrated into a single composite system, the understanding becomes challenging since the light (solar) propagation and liquid (water) transportation would affect each other because water interacts strongly from near-IR to LWIR. Thus, the design of such a composite with optimum cooling power requires a fundamental understanding of the interaction between evaporative and radiative cooling in the same system. The optofluidic properties of such a system should be carefully designed to achieve rational management of light and water transport, which ideally should be adaptive to varying weather conditions.

Herein, we achieved an ultrahigh cooling power of ∼350 W/m^2 with integrated cooling strategies in a rationally designed hydrogel. We carefully engineered the optofluidic properties of a hydrogel to concurrently achieve excellent solar reflection, heat isolation, LWIR emission, and water evaporation. Effective subambient passive cooling (up to 6 °C below ambient temperature) is achieved in tropical Singapore, while a better cooling performance (up to 10 °C) is observed in other regions, including Illinois in the USA and Paris in France. Our integrated passive cooler (IPC) maintains a stable temperature adaptively regardless of the fluctuating ambient conditions, attributed to the sensitive self-tuning of evaporative behavior depending on incident energy. An experimental comparison shows that the IPC has 6−10 times higher cooling potential (power output is solar intensity dependent) in a tropical climate than that of a state-of-the-art radiative cooler, while consuming 200 times less water to achieve cooling performance comparable to that of a conventional spray cooling system. Our in situ radiative cooling study under controlled hydration levels and ambient humidity shed light on the interaction between radiative and evaporative cooling in the system. Beyond working as a single composite layer, IPC is proved to have broad engineering potential, serving as a functional composite privileged by its facile fabrication, providing insights for next-generation passive cooler design.

Design of IPC with Desired Optofluidic Properties. We hypothesize achieving subambient passive cooling by rational integration of various strategies in a single composite material through one-step formation to tackle the issues above.

https://doi.org/10.1021/acs.nanolett.3c03694
Nano Lett. XXXX, XXX, XXX−XXX

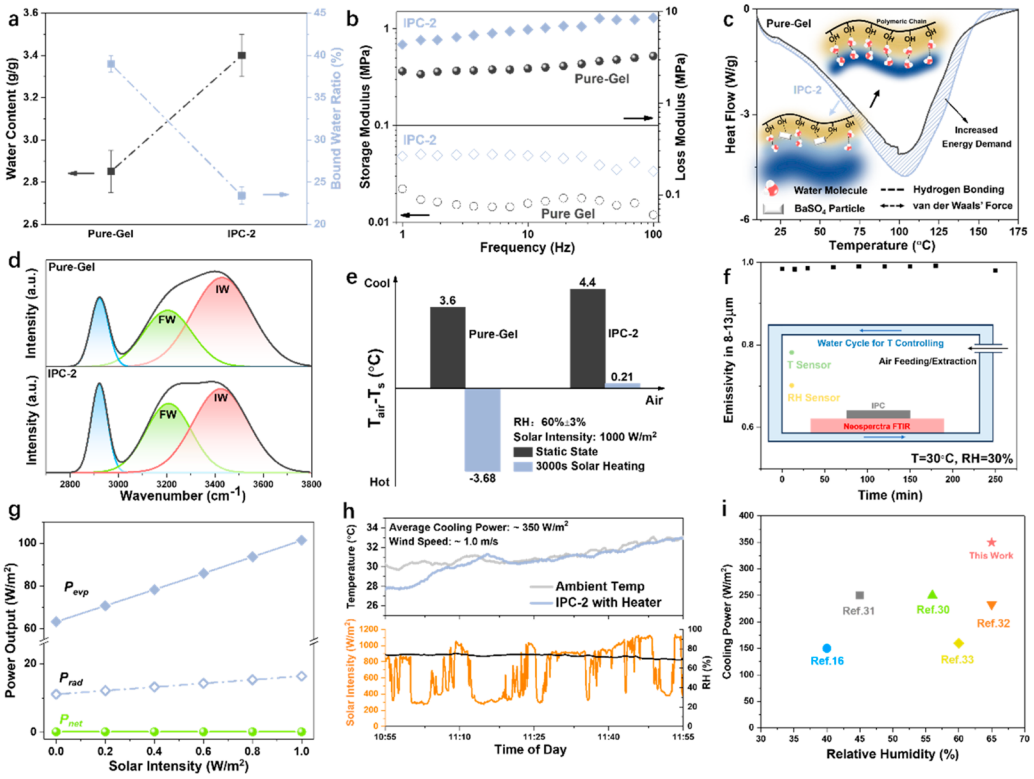

Figure 2. Passive cooling mechanisms and performance evaluation of IPC. (a) Comparison of water content and bound water ratio within Pure-Gel and IPC-2. (b) Storage and loss moduli of Pure-Gel and IPC-2. (c) DSC thermogram of water evaporation within Pure-Gel and IPC-2. Insets: schematic structures. (d) Raman OH stretching mode of Pure-Gel (upper) and IPC-2 (lower). (e) Indoor evaporative cooling comparison and temperature increase comparison (under solar illumination) between Pure-Gel and IPC-2. (f) In situ emissivity change along continuous water evaporation in a constant environment revealing the possible coexistence of radiative and evaporative cooling within an individual panel. The inset is a schematic illustration of the test bed. (g) Solar intensity dependent output power density by evaporative (P_{evp}) and radiative (P_{rad}) cooling and the power difference (P_{net}) between incident and output energies of IPC-2, which indicates the near static state and accuracy of the thermal dynamic model. (h) Experimental cooling power test of IPC-2 in a typical sunny day in Singapore (tropical climate). (i) Cooling power comparison among IPC-2 and state-of-art multifeature passive coolers under different RHs.

A structural media that is water maintainable (for evaporative cooling), thermally isolative, solar reflective, and LWIR emissive (for radiative cooling) could act as such an IPC.

Water has negligible ultraviolet−visible−near-infrared (UV−vis-NIR) light (300−1300 nm, which accounts for ∼87.5% of total solar energy) absorption but partial short-wave IR (1300−2500 nm) absorption in the solar spectrum.[17] Thus, the optical regulation in an IPC should reject most solar energy similarly to a conventional PRC. To cover a tropical climate, UV reflection should be enhanced compared to that of a conventional PRC. The total reflection of NIR absorbance is challenging; it only accounts for ∼3% solar energy. With complementary simultaneous evaporation cooling, NIR absorption-induced heating can be well compensated. Besides, the structural design should balance the water maintenance and light scattering, because the stored water leads to weakened light scattering due to a reduced refractive index difference between water and the polymeric matrix, while additive solar scattering also affects water maintanence.[18] To this end, a rationally designed hydrogel consisting of a porous polymeric matrix that effectively regulates water storage, transportation, and evaporation through multistate water bonding is suitable for an IPC framework.[19,20]

Water evaporation, leading to evaporative cooling, can be triggered by several factors including solar irradiance, ambient temperature, relative humidity, wind, etc. Atmospheric radiation, solar illumination, and parasitic heat transfer can be compensated well by evaporative cooling power generated by water evaporation. Apart from the incident energy, water evaporation continuously takes away internal thermal energy of a passive cooler under the vapor pressure difference between an IPC and the ambient environment. Such a water evaporation driven by unsaturated vapor pressure is inevitable as long as the relative humidity is not 100% regardless of other climate conditions, leading to constant heat reduction. Most important, this environmental-condition-dependent behavior of water evaporation leads to an adaptive cooling performance and thus a steady temperature profile.

Optical and Structural Characterizations of IPC. An IPC (Experimental Section in the Supporting Information) was synthesized by dispersing $BaSO_4$ particles (BSPs) into a typical PVA hydrogel matrix. As illustrated in Figure 1a, PVA polymeric chains (gray) tightly stabilize water (light blue) through hydrogen bonding, where BSPs (white) within the polymeric network backscatter UV−vis−NIR light (300−1300 nm, ∼87.5% of solar energy).[17,21] OH bending (water and PVA) and SO_4 vibration endow the IPC with high IR emissivity to facilitate radiative cooling. Compared to bare surfaces (Figure 1b), the IPC-coated surface can effectively minimize incoming solar heat gain. The active cooling demand (ACD) is the energy required to maintain a constant indoor temperature by an active cooling system (e.g., air conditioner),

https://doi.org/10.1021/acs.nanolett.3c03694
Nano Lett. XXXX, XXX, XXX−XXX

which is taken as a comparison factor to evaluate cooling performance.

A theoretical light scattering analysis suggests that UV−vis−NIR light is strongly scattered by the added BSPs with diameters of 0.3−0.4 μm, resulting in efficient optical regulation (Figure 1c and Supplementary Note 1). Glutaraldehyde cross-links polymer chains through an acetal reaction while electrostatic force between $-SO_4$ and −OH anchors the interpenetrated BSPs (Figure 1d and Figure S2 and Supplementary Note 2).[22,23] BSPs introduce strong Mie scattering to UV−vis light (Figure 1e and Figure S3a−d), leaving negligible transmission (Figure 1f) through IPC-2 (Experimental Section and Supplementary Note 3). The strong visible-light backscattering leads to a white appearance (Figure 1g, upper panel). The optical feature of IPC is proven to be stable through a dry−wet process, where negligible reflectance change is observed after full recovery through water absorption (Figure S3e). Moreover, IPC-2 exhibits high LWIR emissivity (~94%, Figure 1h) in a dry state (freeze-drying), attributed to the intrinsic vibration of OH and SO_4 bonds. Notably, 97% LWIR emittance benchmarks that of the state-of-the-art PRC.[24−27] Thanks to these superior parameters favorable to passive cooling, IPC-2 shows outstanding subambient cooling performance even without effective thermal insulation under extreme climate conditions (~1045 W/m^2, RH ~60%), as revealed by the IR image in Figure 1g (lower panel).

Compared to the reference of a pure hydrogel (pure-Gel), IPC-2 exhibits 19% higher water content with 40% less bound water, providing 51% more evaporable water (Figure 2a and Figure S4 and Supplementary Note 4). Though the hydroxyl groups on polymeric chains are partially occupied by bound BSPs via electrostatic force (Figure S2), the expanded porous matrix owing to a steric hindrance effect (SHE) arising from BSPs enhances intermediate/free water storage compared to pure-Gel (Figure S5). Dynamic mechanical analysis reveals that IPC possesses enhanced mechanical strength (storage modulus) benefiting from the interpenetrated BSPs, and the increased loss modulus in turn suggests a significant SHE, further indicating a balance between mechanical and swelling properties (Figure 2b and Supplementary Note 5).[19,28] It is worth noting that IPC is proved to be mechanically stable through repeated water cycles, where both the storage and loss modulus are maintained during a dry−wet state transition experiment (Figure S3f). The decreased connections among polymeric chains arising from the SHE further impedes inner heat transfer, leading to lowered thermal conductivity at both saturated and dry states, favoring passive cooling.[26] (Figure S6 and Supplementary Note 6).[29] The endothermic curve (Figure 2c and Figure S7) indicates distinct evaporative behaviors in IPC-2 compared to pure water, where the drastically broadened peak suggests the presence of bound and intermediate water with a stronger hydrogen bonding interaction.[19] The presence of $BaSO_4$ theoretically (Figure S8 and Supplementary Note 7) leads to a stronger system viscosity compared to that of the pure hydrogel, restricting the dynamics of the water network. Meanwhile, $BaSO_4$−water hydrogen bonds have an ~1.5 times longer lifetime and ~5 times higher binding energy (Figure S9) compared to a water−water hydrogen bond, which hinders the formation of an ordered hydrogen bonding network and leads to higher evaporative enthalpy. A thermal analysis (Figure S10f and model details in Supplementary Note 8) clearly reveals that higher evaporative enthalpy is more favorable to cooling since it can also prolong the cooling time. It is worth noting that both mass and thermal transfer are considered in the theoretical model, which is further validated by experimental results, proving its accuracy. The Raman OH stretching mode shows a lower intermediate/free water (IW/FW) ratio in IPC-2 than in Pure-Gel (Figure 2d and Figure S11 and Supplementary Note 9), suggesting less intermediate water content that leads to a higher evaporative enthalpy in the IPC (Figure 2c). The distinct water states fundamentally differentiate the evaporation behavior of water in IPC from that of normal water, which leads to fine control of evaporation behavior dynamically, resulting in a drastically increased evaporative cooling efficiency. Specifically, with the same amount of evaporated water, IPC-2 saves 92% ACD on a sunny day (solar intensity, 1000 W/m^2; RH, 60%; wind speed, ~1.5 m/s). Moreover, IPC-2 shows a 50% longer cooling cycle than normal water, indicating a much more sustainable cooling effect (Figure S12). Cooling performances are compared between IPC and conventional spray cooling in Figure S13 (Supplementary Note 10). Though the surficial temperature of bare aluminum (Al) decreased by 25 °C under a continuous water spray (13.8 mL/(m^2 s)), its temperature is still ~2 °C above that of IPC-2 under high solar irradiance (800−1000 W/m^2). Moreover, the fluctuating Al temperature is in obvious contrast to the stable temperature of the IPC. Importantly, the water consumption is >200 times higher than that of IPC-2 (~0.05 mL/(m^2 s)). It is worth noting that the surface temperature rose immediately after most of the water evaporated, suggesting nonsustainable cooling by spraying water.

IPC Cooling Capability Evaluation. The lower indoor (to exclude radiative cooling) temperature of IPC-2 than that of Pure-Gel (Figure 2e and Figure S14 and Supplementary Note 11) proves the effectiveness of enhanced fluidic properties on evaporative cooling. Apparently, 3000 sun solar illumination (1000 W/m^2) heated Pure-Gel to 3.68 °C above ambient temperature. In contrast, IPC-2 remained at a subambient temperature. Notably, the thickness of IPC is negligible in affecting surface temperatures (Figure S15) but is responsible for increasing the length of each cooling cycle (Figures S16 and S17).

An in situ study was conducted to investigate the interaction between radiation and evaporation, which helps to understand the rationality of the multifunction surface design in the IPC. It is clear that continuous water evaporation negligibly affects surficial emissivity within the atmospheric window, indicating the coexistence of excellent radiative and evaporative features (Figure 2f). Correspondingly, a near-steady-state thermal analysis derived net power density (sunlight and environment) shows that the IPC-2 coating significantly reduces the ACD of rooftop by a >81.5% to maintain a comfortable indoor temperature (25 °C). Compared to the ideal PRC, IPC-2 leads to a lower ACD when it is thicker than 6 mm and possesses the potential to fully minimize the ACD when it gets thicker over a long run (Figure S18a).[24,25] Heat isolation is enhanced when IPC thickness increases, leading to a more effective rejection of incoming atmospheric thermal energy. Though the ACD is reduced effectively, the cooling efficiency (the ratio of cooling power density to thickness) starts to decrease because thickness plays a negligible role in decreasing solar heat gain. The intersection of cooling efficiency and reciprocal of ACD indicates 10 mm to be an appropriate thickness for outdoor

https://doi.org/10.1021/acs.nanolett.3c03694
Nano Lett. XXXX, XXX, XXX−XXX

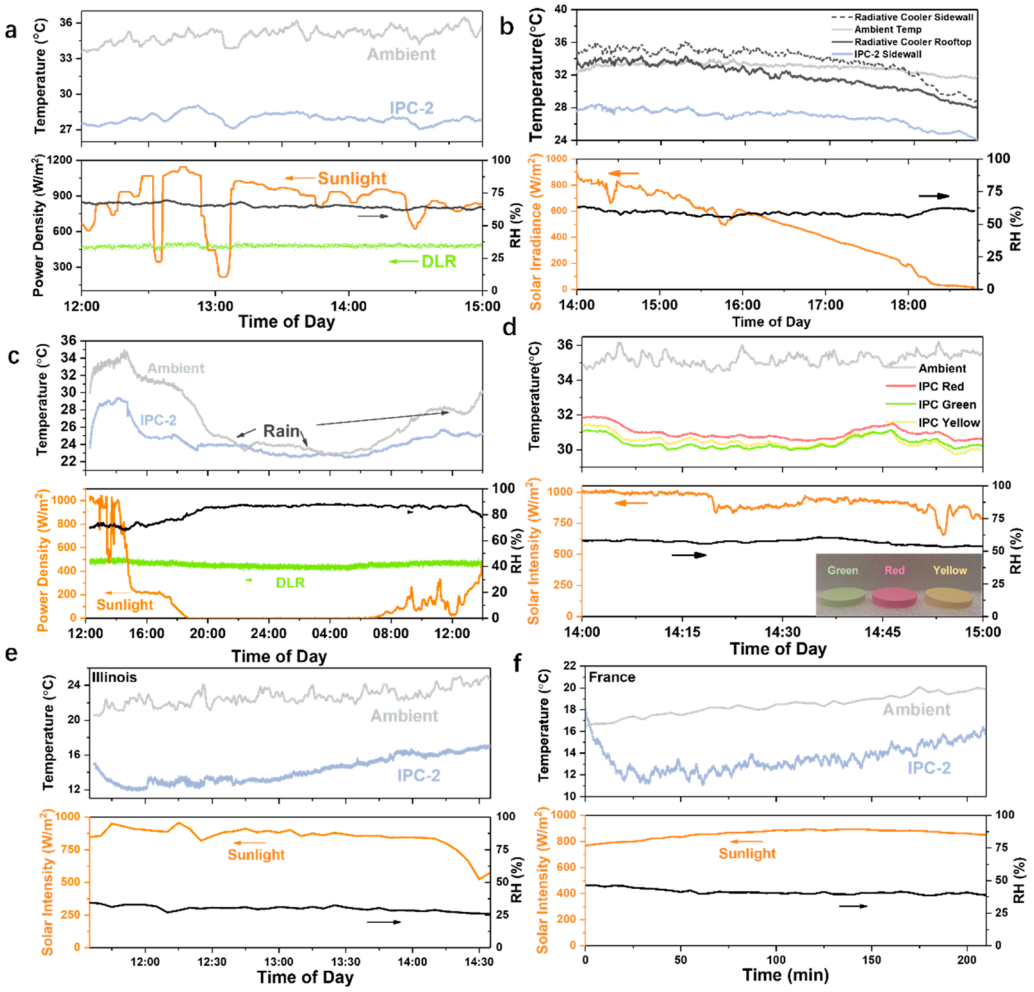

Figure 3. Cooling performances of IPC-2 under various weather conditions. (a) Outdoor cooling performance of IPC-2 in a typical sunny daytime in Singapore. (b) Outdoor cooling performance of IPC-2 compared with the state-of-the-art PRC at different faces. (c) Day-long temperature recording of ambient air and passive cooler, with no water replenishment during the test. The tested IPC-2 sample has dimensions of 25 cm (L) × 20 cm (W) × 4 mm (T). (d) Outdoor subambient cooling achieved by colored IPC-2 samples (lower panel inset), indicating effectiveness of the integrated cooling structure. (e) Outdoor cooling performance test of IPC-2 at University of Illinois Urbana—Champaign in Illinois, United States on May 25th, 2023. (f) Outdoor cooling performance test of IPC-2 at Sorbonne University Pierre and Marie Curie Campus in Paris, France, on May 25th, 2023.

cooling (under ambient conditions for Figure S18a) with acceptable ACD without apparently compromising cooling efficiency (Figure S18b).

To further evaluate the cooling capability of the IPC, the theoretical energy output from the thermodynamic model is provided (Figure 2g). Obviously, the evaporative energy consumption varies significantly with solar irradiance, while the radiative energy output slightly changes and remains at a low level due to the unfavorable atmospheric hindrance (high RH). Notably, ~2−5% solar absorbance totally compensates for the radiative cooling power of the state-of-the-art radiative cooler in the tropics when the solar intensity reaches 1000 W/m^2. As such, no subambient passive cooling could be achieved by LWIR radiation alone. Interestingly, the higher and stable cooling power exhibited by the IPC under stronger sunlight is obviously different from that of a conventional radiative cooler, which indicates its high performance and adaptive cooling feature. As such, the IPC automatically tunes the contributions of evaporative cooling to maintain a stable temperature, leading to adaptive passive cooling under various conditions regardless of the varying weather or indoor/outdoor conditions. In comparison with recent reported works, we experimentally achieved a record-high cooling power of approximately 350 W/m^2 on a typical sunny day, which is superior to those of state-of-the -art passive coolers with various designs (Figure 2h,i).[16,30−33] In comparison with the reported multilayer structure, direct optical modification of the hydrogel matrix ensured mechanical stability since a interfacial adhesion problem between the radiative and evaporative layers may occur when the hydrogel matrix suffers great water loss. The higher cooling power of IPC-2 is attributed to a larger evaporative surface without covering a layer of a radiative cooler.

Cooling Performance Test. 24 h indoor cooling (~3 °C below ambient temperature) was achieved with 4 mm thick IPC-2 (Figure S19), in apparent contrast to a PRC that does not work indoors due to a blocked atmospheric window and indicated the effectiveness of evaporative cooling driven by unsaturated vapor pressure. Strikingly, outdoor cooling with ~6 °C below ambient temperature in the early afternoon of a sunny day (solar irradiance up to 1140 W/m^2 at RH > 60%) was achieved, in apparent contrast to the near-ambient

https://doi.org/10.1021/acs.nanolett.3c03694
Nano Lett. XXXX, XXX, XXX−XXX

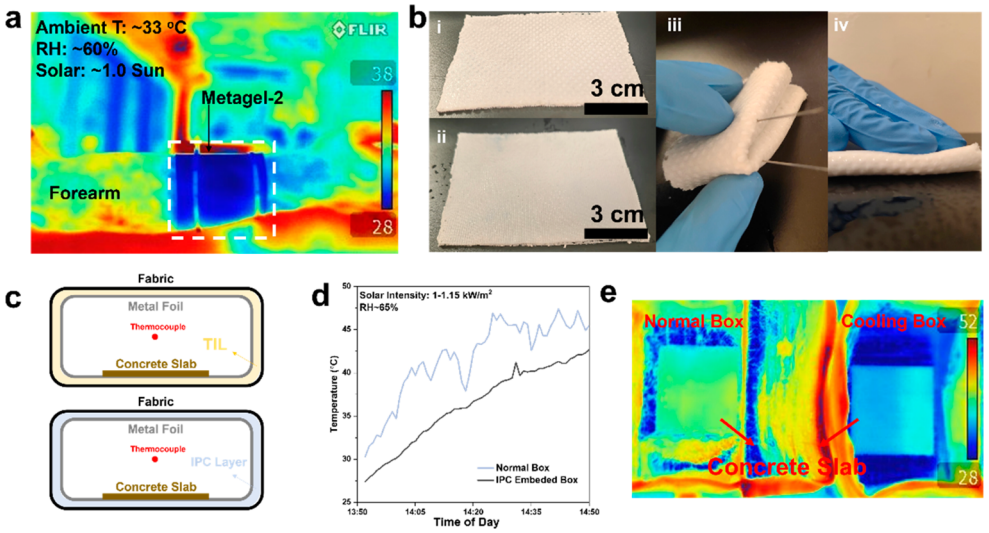

Figure 4. Demonstration of promising applications and engineering potential of IPC. (a) IR image showing outdoor subambient cooling of IPC on human skin (the same sample as that in Figure S22c). (b) Demonstration of direct composition between IPC and commercial fabric (10 cmL × 7 cmW × 4 mmT). (c) Schematic illustration of IPC as a composite cooling layer in a commercial food box. (d) Temperature recording of IPC cooling for a commercial food box. (e) IR image of concrete slabs inside two food boxes at 2:50 pm, August 4th, 2022, in Singapore (Figure 4d).

temperature of the state-of-the-art PRC under similar ambient conditions (Figure 3a,b and Figure S20a and Supplementary Note 12). Moreover, a greater contrastive cooling performance was demonstrated between a commercial radiative cooling paint (Nippon Solareflect Si) and the IPC, where the optical performances are quite similar between each other (comparable solar reflectance of ~88%, Figure S20b−d).[15] This directly reveals the cooling contribution from evaporative behavior. Moreover, the temperature of the cooled substrate remained very stable at 28 ± 0.5 °C, effectively avoiding the drastic temperature variation caused by fluctuating solar heat gain (Figure 3a). It is worth noting that a state-of-the-art PRC shows 2 °C higher temperature on sidewalls than that on a rooftop, which is at near-ambient temperature (Figure 3b) due to the halved radiation angle and increased incident thermal energy from the surroundings.[34] In contrast, IPC-2 shows 4−6 °C subambient temperature on sidewalls and a rooftop, which are attributed to the nondirectional feature of evaporative behavior. It is proved that a high NIR reflective material for sidewall application leading to inevitable thermal discomfort would be alleviated by the IPC concept that partial solar energy would be directly transferred into inner energy of water vapor through a phase change process due to solar absorption of interfacial water.[35] Though water evaporation is strongly affected by relative humidity, nighttime subambient (3−5 °C) cooling was still achieved despite a high RH of ~80% (Figure S21). To further illustrate the adaptive cooling feature and durability of the IPC cooler, we conducted a 24 h continuous field test, during which various atmospheric conditions appeared including strong/weak sunshine, raining, cloud, and nighttime weather conditions. As shown in Figure 3c, 6 °C cooling was achieved with intense sunlight in the daytime. Even when it was raining, the passive cooler still reached a subambient temperature, and the temperature fluctuation was much smaller than that of the air temperature due to its adaptive cooling mechanism. This indicates that the IPC exhibits superior sustainable cooling performance. PRCs typically appear white to reflect the entire visible solar spectrum and colored PRCs that have broader applications are preferred. Coloring inevitably results in increased solar heat gain that raises surface temperatures to above ambient.[36−38] In contrast, colored IPC-2 still shows a subambient (~3.5 °C, Figure 3d and Figure S22) cooling performance under ~1000 W/m^2 thanks to the rationally integrated cooling strategies.

Since the tropical climate is the most challenging for passive cooling, and our IPC cooler works well in tropical Singapore, we anticipate it would work equally well or better in other climates. To verify this, the cooling performance of the IPC was measured on two different continents (America and Europe). Recorded temperature profiles in Illinois, USA (Figure 3e) and Paris, France (Figure 3f) indicate a subambient cooling performance up to 10 °C with the IPC. These results suggest a generic cooling performance and excellent adaptivity.

Next, we further evaluated the applicable potential of the IPC design. IPC holds promise as cooling pads due to its nonhazardous nature (Figure S23a) and excellent mechanical flexibility and strength. 2 mm thick IPC-2 can be conformally attached to the skin (Figure 4a and Figure S22b−d, resulting in an ~28 °C skin temperature despite the high ambient temperature (~33 °C) under 1 sun irradiation. Moreover, IPC could be easily composited into a commercial fabric through a facile one-step cross-linking process (Figure 4b-i,ii). The soaked fabric filled with an IPC precursor spontaneously forms a porous network within the framework, holding its original appearance but gaining a cooling capability as an IPC. As shown, the composited fabric-IPC exhibits great flexibility and antipuncture properties (Figure 4b-iii). Thanks to the abundant hydrogen bonding interactions between IPC and fabric bones, strong adhesion is achieved with supreme mechanical performance, which is further confirmed by the lack of falling off under strong bending and pressing (Figure 4b-iv). The demonstrated composition integrated with a commercial fabric provides better human comfort. Beyond this, we demonstrated an effective cooling performance in a commercial food box, where the IPC serves as an interlayer (replacing a thermal isolative layer) to provide a cooling function (Figure 4c). An obvious temperature reduction of up

https://doi.org/10.1021/acs.nanolett.3c03694
Nano Lett. XXXX, XXX, XXX−XXX

to 7 °C was recorded under strong solar illumination outdoors, where the IR images of concrete slabs (taken when the food box is open) further prove the cooled atmosphere even in the absence of inner convection (Figure 4d,e). Additionally, the IPC shows excellent fire retardant performance (Figure S24 and Supplementary Note 13) thanks to the contained water and added BSPs.[39] Videos 1 and 2 clearly show that the inner structure of IPC was maintained after long-term burning from both vertical and parallel directions; only a thin char layer formed at the surface. Altogether, IPC opens a route for adaptive passive cooling for various potential applications in a tropical climate and beyond (Supplementary Note 14).

We have successfully engineered a hydrogel-based IPC composite that provides a solution to the subambient passive cooling challenge in harsh tropical climates. Incorporating a variety of mechanisms such as high solar reflection, heat insulation, long-wave infrared (LWIR) radiation, and evaporative cooling, the composite delivers a remarkable cooling power of 350 W/m^2 and achieves 4−8 °C subambient passive cooling in tropical climates. Demonstrating excellent adaptability to fluctuating ambient conditions, our IPC cooler maintains stable subambient temperatures despite changing weather conditions. It exhibits superior cooling performances in climates beyond the tropics, recording up to 10 °C subambient temperatures in America and Europe. Additionally, the IPC can work as a colored passive cooler which could achieve subambient cooling under strong sunlight, which is challenging for a pure radiative cooler. Given its cost-effectiveness, adaptability, abundant choice of spectral regulation agents, and high engineering flexibility, the IPC cooler holds great promise for wide application across various climates.

■ ASSOCIATED CONTENT

Supporting Information

The Supporting Information is available free of charge at https://pubs.acs.org/doi/10.1021/acs.nanolett.3c03694.

- Char test of the IPC under a vertical condition (MP4)
- Char test of the IPC under a parallel condition (MP4)
- Details of sample preparation, theoretical simulations, and supporting experimental results (PDF)

■ AUTHOR INFORMATION

Corresponding Author

Hong Li − *School of Mechanical and Aerospace Engineering and School of Electric and Electronic Engineering, Nanyang Technological University, Singapore 639798, Singapore; CINTRA CNRS/NTU/THALES, UMI 3288, Singapore 637553, Singapore;* orcid.org/0000-0002-6975-7787; Email: ehongli@ntu.edu.sg

Authors

Jipeng Fei − *School of Mechanical and Aerospace Engineering, Nanyang Technological University, Singapore 639798, Singapore*

Di Han − *School of Mechanical and Aerospace Engineering, Nanyang Technological University, Singapore 639798, Singapore*

Xuan Zhang − *Department of Energy and Power Engineering, School of Mechanical Engineering, Beijing Institute of Technology, Beijing 100081, People's Republic of China*

Ke Li − *Institute of Materials Research and Engineering, Agency for Science, Technology and Research, Singapore 138634, Singapore; School of Materials Science and Engineering, Nanyang Technological University, Singapore 639798, Singapore;* orcid.org/0000-0002-3140-3983

Nicolas Lavielle − *Univ Gustave Eiffel, CNRS, ESYCOM, Marne la Vallée F77454, France;* orcid.org/0000-0001-5842-2992

Kai Zhou − *Department of Mechanical Science and Engineering, University of Illinois at Urbana−Champaign, Urbana, Illinois 61801, United States;* orcid.org/0000-0003-4653-6436

Xingli Wang − *CINTRA CNRS/NTU/THALES, UMI 3288, Singapore 637553, Singapore*

Jun Yan Tan − *School of Mechanical and Aerospace Engineering, Nanyang Technological University, Singapore 639798, Singapore*

Jianwei Zhong − *Pillar of Engineering Product Development, Singapore University of Technology and Design, Singapore 487372, Singapore;* orcid.org/0000-0001-6198-868X

Man Pun Wan − *School of Mechanical and Aerospace Engineering, Nanyang Technological University, Singapore 639798, Singapore*

Elyes Nefzaoui − *Univ Gustave Eiffel, CNRS, ESYCOM, Marne la Vallée F77454, France*

Tarik Bourouina − *Univ Gustave Eiffel, CNRS, ESYCOM, Marne la Vallée F77454, France; CINTRA CNRS/NTU/THALES, UMI 3288, Singapore 637553, Singapore;* orcid.org/0000-0003-2342-7149

Shuzhou Li − *School of Materials Science and Engineering, Nanyang Technological University, Singapore 639798, Singapore;* orcid.org/0000-0002-2159-2602

Bing Feng Ng − *School of Mechanical and Aerospace Engineering, Nanyang Technological University, Singapore 639798, Singapore;* orcid.org/0000-0001-8112-1151

Lili Cai − *Department of Mechanical Science and Engineering, University of Illinois at Urbana−Champaign, Urbana, Illinois 61801, United States;* orcid.org/0000-0003-1222-248X

Complete contact information is available at: https://pubs.acs.org/10.1021/acs.nanolett.3c03694

Author Contributions

△J.L. and D.H. contributed equally to this work.

Author Contributions

J.F. and H.L. conceptualized the idea of and designed experiments. J.F. and D.H. conducted sample fabrication and characterization. K.L. and S.L. conducted DFT and MD simulation work. D.H. and X.Z. conducted computational work for theoretical analysis. S.-W.K., X.W., N.L., E.N., K.Z., J.Y.T., and J.Z. helped conduct material characterizations. M.P.W., B.F.N., L.C., T.B., and H.L. provided financial and equipment support on the conduction of experiments. J.F. and X.Z. drafted the manuscript, which was reviewed by all coauthors. The whole work was supervised by H.L.

Notes

The authors declare the following competing financial interest(s): J.F. and H.L. are inventors on a patent application related to this work, filed by Nanyang Technological University Singapore (application no. 10202113624U). The authors declare no other competing interests.

https://doi.org/10.1021/acs.nanolett.3c03694
Nano Lett. XXXX, XXX, XXX−XXX

■ ACKNOWLEDGMENTS

This work was supported by Nanyang Technological University under an NAP award (M408050000) and the Singapore Ministry of Education Tier 1 program (RG58/21 & RG97/18 (S)). The authors acknowledge the Facility for Analysis, Characterization, Testing and Simulation (FACTS), Nanyang Technological University Singapore, for use of electron microscopy and X-ray facilities.

■ REFERENCES

(1) Goldthau, A.; Hughes, L. Protect global supply chains for low-carbon technologies. *Nature* **2020**, *585*, 28−30.
(2) Hertwich, E. G.; Gibon, T.; Bouman, E. A.; Arvesen, A.; Suh, S.; Heath, G. A.; Bergesen, J. D.; Ramirez, A.; Vega, M. I.; Shi, L. Integrated life-cycle assessment of electricity-supply scenarios confirms global environmental benefit of low-carbon technologies. *Proc. Natl. Acad. Sci. U.S.A.* **2015**, *112* (20), 6277−6282.
(3) Wakerley, D.; Lamaison, S.; Ozanam, F.; Menguy, N.; Mercier, D.; Marcus, P.; Fontecave, M.; Mougel, V. Bio-inspired hydrophobicity promotes CO2 reduction on a Cu surface. *Nat. Mater.* **2019**, *18* (11), 1222−1227.
(4) Yang, S.; Lin, X.; Lewis, W.; Suyetin, M.; Bichoutskaia, E.; Parker, J. E.; Tang, C. C.; Allan, D. R.; Rizkallah, P. J.; Hubberstey, P.; et al. A partially interpenetrated metal−organic framework for selective hysteretic sorption of carbon dioxide. *Nat. Mater.* **2012**, *11* (8), 710−716.
(5) Chua, K. J.; Chou, S. K.; Yang, W.; Yan, J. Achieving better energy-efficient air conditioning−a review of technologies and strategies. *Appl. Energy* **2013**, *104*, 87−104.
(6) Taleb, H. M. Using passive cooling strategies to improve thermal performance and reduce energy consumption of residential buildings in UAE buildings. *Front. Archit. Res.* **2014**, *3* (2), 154−165.
(7) Raman, A. P.; Anoma, M. A.; Zhu, L.; Rephaeli, E.; Fan, S. Passive radiative cooling below ambient air temperature under direct sunlight. *Nature* **2014**, *515* (7528), 540−4.
(8) Zeng, S.; Pian, S.; Su, M.; Wang, Z.; Wu, M.; Liu, X.; Chen, M.; Xiang, Y.; Wu, J.; Zhang, M.; Cen, Q.; Tang, Y.; Zhou, X.; Huang, Z.; Wang, R.; Tunuhe, A.; Sun, X.; Xia, Z.; Tian, M.; Chen, M.; Ma, X.; Yang, L.; Zhou, J.; Zhou, H.; Yang, Q.; Li, X.; Ma, Y.; Tao, G. Hierarchical-morphology metafabric for scalable passive daytime radiative cooling. *Science* **2021**, *373* (6555), 692−696.
(9) Mandal, J.; Fu, Y.; Overvig, A. C.; Jia, M.; Sun, K.; Shi, N. N.; Zhou, H.; Xiao, X.; Yu, N.; Yang, Y. Hierarchically porous polymer coatings for highly efficient passive daytime radiative cooling. *Science* **2018**, *362* (6412), 315−319.
(10) Zhan, Z.; ElKabbash, M.; Li, Z.; Li, X.; Zhang, J.; Rutledge, J.; Singh, S.; Guo, C. Enhancing thermoelectric output power via radiative cooling with nanoporous alumina. *Nano Energy* **2019**, *65*, 104060.
(11) Zhai, Y.; Ma, Y.; David, S. N.; Zhao, D.; Lou, R.; Tan, G.; Yang, R.; Yin, X. Scalable-manufactured randomized glass-polymer hybrid metamaterial for daytime radiative cooling. *Science* **2017**, *355* (6329), 1062−1066.
(12) Li, D.; Liu, X.; Li, W.; Lin, Z.; Zhu, B.; Li, Z.; Li, J.; Li, B.; Fan, S.; Xie, J.; Zhu, J. Scalable and hierarchically designed polymer film as a selective thermal emitter for high-performance all-day radiative cooling. *Nat. Nanotechnol.* **2021**, *16* (2), 153−158.
(13) Han, D.; Ng, B. F.; Wan, M. P. Preliminary study of passive radiative cooling under Singapore's tropical climate. *Sol. Energy Mater. Sol. Cells* **2020**, *206*, 110270.
(14) Kim, S.; Shang, W.; Moon, S.; Pastega, T.; Lee, E.; Luo, T. High-Performance Transparent Radiative Cooler Designed by Quantum Computing. *ACS Energy Lett.* **2022**, *7* (12), 4134−4141.
(15) Han, D.; Fei, J.; Mandal, J.; Liu, Z.; Wan, M. P.; Li, H.; Raman, A. P.; Ng, B. F. Highly Reflective Polymeric Coating for Passive Radiative Cooling Under Tropical Climate. *Sol. Energy Mater. Sol. Cells* **2022**, *240*, 111723.
(16) Feng, C.; Yang, P.; Liu, H.; Mao, M.; Liu, Y.; Xue, T.; Fu, J.; Cheng, T.; Hu, X.; Fan, H. J.; Liu, K. Bilayer porous polymer for efficient passive building cooling. *Nano Energy* **2021**, *85*, 105971.
(17) Ustin, S. L.; Riaño, D.; Hunt, E. R. Estimating canopy water content from spectroscopy. *Isr. J. Plant Sci.* **2012**, *60* (1), 9−23.
(18) Mandal, J.; Jia, M.; Overvig, A.; Fu, Y.; Che, E.; Yu, N.; Yang, Y. Porous Polymers with Switchable Optical Transmittance for Optical and Thermal Regulation. *Joule* **2019**, *3* (12), 3088−3099.
(19) Zhou, X.; Guo, Y.; Zhao, F.; Shi, W.; Yu, G. Topology-Controlled Hydration of Polymer Network in Hydrogels for Solar-Driven Wastewater Treatment. *Adv. Mater.* **2020**, *32* (52), No. e2007012.
(20) Zhou, X.; Zhao, F.; Guo, Y.; Zhang, Y.; Yu, G. A hydrogel-based antifouling solar evaporator for highly efficient water desalination. *Energy Environ. Sci.* **2018**, *11* (8), 1985−1992.
(21) Fei, J.; Ding, B.; Koh, S. W.; Ge, J.; Wang, X.; Lee, L.; Sun, Z.; Yao, M.; Chen, Y.; Gao, H.; et al. Mechanistic Investigation of Electrostatic Field-Enhanced Water Evaporation. *Adv. Sci.* **2021**, *8* (18), 2100875.
(22) Ramaswamy, V.; Vimalathithan, R.; Ponnusamy, V. Synthesis and characterization of BaSO4 nano particles using micro emulsion technique. *Adv. Appl. Sci. Res.* **2010**, *1* (3), 197−204.
(23) El Khoury, Y.; Hellwig, P. Far infrared spectroscopy of hydrogen bonding collective motions in complex molecular systems. *Chem. Commun. (Camb)* **2017**, *53* (60), 8389−8399.
(24) Li, X.; Peoples, J.; Huang, Z.; Zhao, Z.; Qiu, J.; Ruan, X. Full Daytime Sub-ambient Radiative Cooling in Commercial-like Paints with High Figure of Merit. *Cell Rep. Phys. Sci.* **2020**, *1* (10), 100221.
(25) Wang, T.; Wu, Y.; Shi, L.; Hu, X.; Chen, M.; Wu, L. A structural polymer for highly efficient all-day passive radiative cooling. *Nat. Commun.* **2021**, *12* (1), 365.
(26) Zhong, H.; Li, Y.; Zhang, P.; Gao, S.; Liu, B.; Wang, Y.; Meng, T.; Zhou, Y.; Hou, H.; Xue, C.; Zhao, Y.; Wang, Z. Hierarchically Hollow Microfibers as a Scalable and Effective Thermal Insulating Cooler for Buildings. *ACS Nano* **2021**, *15* (6), 10076−10083.
(27) Zhao, H.; Sun, Q.; Zhou, J.; Deng, X.; Cui, J. Switchable Cavitation in Silicone Coatings for Energy-Saving Cooling and Heating. *Adv. Mater.* **2020**, *32* (29), No. e2000870.
(28) Zhou, X.; Zhao, F.; Guo, Y.; Rosenberger, B.; Yu, G. Architecting highly hydratable polymer networks to tune the water state for solar water purification. *Sci. Adv.* **2019**, *5* (6), eaaw5484.
(29) Zhou, J.; Lin, S.; Zeng, H.; Liu, J.; Li, B.; Xu, Y.; Zhao, X.; Chen, G. Dynamic intermolecular interactions through hydrogen bonding of water promote heat conduction in hydrogels. *Mater. Horiz.* **2020**, *7* (11), 2936−2943.
(30) Li, J.; Wang, X.; Liang, D.; Xu, N.; Zhu, B.; Li, W.; Yao, P.; Jiang, Y.; Min, X.; Huang, Z.; et al. A tandem radiative/evaporative cooler for weather-insensitive and high-performance daytime passive cooling. *Sci. Adv.* **2022**, *8* (32), eabq0411.
(31) Yao, H.; Cheng, H.; Liao, Q.; Hao, X.; Zhu, K.; Hu, Y.; Qu, L. Integrated radiative and evaporative cooling beyond daytime passive cooling power limit. *Nano Res. Energy* **2023**, *2*, No. e9120060.
(32) Xu, L.; Sun, D.-W.; Tian, Y.; Fan, T.; Zhu, Z. Nanocomposite hydrogel for daytime passive cooling enabled by combined effects of radiative and evaporative cooling. *Chem. Eng. J.* **2023**, *457*, 141231.
(33) Yang, M.; Zhong, H.; Li, T.; Wu, B.; Wang, Z.; Sun, D. Phase Change Material Enhanced Radiative Cooler for Temperature-Adaptive Thermal Regulation. *ACS Nano* **2023**, *17* (2), 1693−1700.
(34) Xu, J.; Mandal, J.; Raman, A. P. Broadband directional control of thermal emission. *Science* **2021**, *372* (6540), 393−397.
(35) Yang, J.; Wang, Z.-H.; Kaloush, K. E. Environmental impacts of reflective materials: Is high albedo a 'silver bullet' for mitigating urban heat island? *Renew. Sustain. Energy Rev.* **2015**, *47*, 830−843.
(36) Chen, Y.; Mandal, J.; Li, W.; Smith-Washington, A.; Tsai, C.-C.; Huang, W.; Shrestha, S.; Yu, N.; Han, R. P.; Cao, A.; et al. Colored and paintable bilayer coatings with high solar-infrared reflectance for efficient cooling. *Sci. Adv.* **2020**, *6* (17), eaaz5413.
(37) Sheng, C.; An, Y.; Du, J.; Li, X. Colored Radiative Cooler under Optical Tamm Resonance. *ACS Photonics* **2019**, *6* (10), 2545−2552.

https://doi.org/10.1021/acs.nanolett.3c03694
Nano Lett. XXXX, XXX, XXX−XXX

668 (38) Lee, G. J.; Kim, Y. J.; Kim, H. M.; Yoo, Y. J.; Song, Y. M.
669 Colored, Daytime Radiative Coolers with Thin-Film Resonators for
670 Aesthetic Purposes. *Adv. Opt. Mater.* **2018**, *6* (22), 1800707.
671 (39) Xue, Z.; Zhang, W.; Yan, M.; Liu, J.; Wang, B.; Xia, Y. Pyrolysis
672 products and thermal degradation mechanism of intrinsically flame-
673 retardant carrageenan fiber. *RSC Adv.* **2017**, *7* (41), 25253−25264.

https://doi.org/10.1021/acs.nanolett.3c03694
Nano Lett. XXXX, XXX, XXX−XXX